Available online at www.sciencedirect.com
ScienceDirect
Ceramics International 37 (2011) 175–180
CERAMICS INTERNATIONAL
www.elsevier.com/locate/ceramint

Synthesis and characterization of nanocrystalline merwinite ($Ca_3Mg(SiO_4)_2$) via sol–gel method

Masoud Hafezi-Ardakani [a], Fatollah Moztarzadeh [a,*], Mohammad Rabiee [a], Ali Reza Talebi [b]

[a] *Biomaterials Group, Faculty of Biomedical Engineering (Center of Excellence), Amirkabir University of Technology, Tehran, Iran*
[b] *Research and Clinical Center for Infertility, Department of Anatomy, Shahid Sadoughi University of Medical Sciences, Yazd, Iran*

Received 7 May 2010; received in revised form 18 May 2010; accepted 10 August 2010
Available online 25 September 2010

Abstract

In this research, the synthesis of nanocrystalline merwinite ($2SiO_2$–3CaO–MgO) bioactive ceramic was carried out by the sol–gel method. After crushing, obtained sol–gel derived bioceramic powder pressed uniaxially to produce cylindrical-like pellets, followed by sintering at 1300 °C. Via immersion in simulated body fluid (SBF) for various time intervals, the formation of apatite was characterized. Scanning electron microscopy (SEM), X-ray diffraction analysis (XRD), and Fourier transform infrared spectroscopy (FT-IR) studies were conducted both before and after immersion in SBF. The crystallization temperature of the merwinite was determined by thermal analysis. Attained results confirmed formation of apatite layer within the first day of soaking. Accordingly it can be concluded that merwinite is bioactive and might be used for preparation of implantable biomaterials.

Keywords: Merwinite; Synthesis; Sol–gel; Bioactivity; Hydroxyapatite

1. Introduction

Bone defects are among the most significant worldwide health problem [1,2]. Reconstructions of impaired and defective bone tissue are the part of modern medical practice [3]. Due to several reasons (e.g. immune rejection and limited blood supply) the success rate of traditional repair strategies is low [3]. Following by bioglass introduced by Hench [4,5], numerous bioactive materials showing good surface hydroxyapatite (HA) formation ability have been synthesized [6]. To create nucleation site for HA formation, the simultaneous dissolution of silicates and ensuing formation of Si–OH groups is necessary [7–15]. Most common bioactive materials comprising CaO and SiO_2 follow this mechanism for HA formation on their surfaces. Amorphous phase materials release more Ca ions than crystalline materials which makes them more capable of HA formation [16,17]. Researches have reported excellent bioactivity of some calcium silicate ceramics, such as wollastonite (low temperature, triclinic $CaSiO_3$) [18,19], pseudowollastonite (high temperature, monoclinic $CaSiO_3$) [20–24], diopside ($CaMgSi_2O_6$) [25–27], tricalcium silicate (Ca_3SiO_5) [28], combeite ($Na_2Ca_2Si_3O_9$) [29] and akermanite ($Ca_2MgSi_2O_7$) [30–32].

Merwinite, ($Ca_3MgSi_2O_8$), an orthosilicate, known as a blast furnace slag in cement industries was first described by Larsen and Foshag [33]. The use of merwinite ceramics, which has melting temperature about 1450 °C, as a biomaterial has not been reported until recently [34]. In 2008 merwinite was suggested as a bioceramic with suitable mechanical properties which hold the potential for use as bioactive material for bone repair [34].

The purpose of the present study is to explore the formation of nanocrystalline merwinite *via* sol–gel method. Subsequently, the effect of temperature on the formation of merwinite was evaluated by XRD analysis. Finally, the ability of merwinite ceramic to deposit apatite on its surface in SBF solution was assessed by XRD, FTIR and SEM techniques.

2. Experimental

2.1. Materials and methods

Nanocrystalline merwinite powders were synthesized using the sol–gel method. For this purpose, $Ca(NO_3)_2{\cdot}4H_2O$ (Merck),

* Corresponding author. Tel.: +98 21 64542393; fax: +98 21 64542387.
E-mail addresses: moztarzadeh@aut.ac.ir (F. Moztarzadeh), mrabiee@aut.ac.ir (M. Rabiee).

0272-8842/$36.00
doi:10.1016/j.ceramint.2010.08.034

Table 1
Ion concentration of SBFs and human blood plasma (mM).

	Na^+	Mg^{2+}	K^+	Ca^{2+}	Cl^-	HCO_3^-	HPO_4^{2-}	SO_4^{2-}
Human blood plasma	142.0	1.5	5.0	2.5	103.0	27.0	1.0	0.5
Original SBF	142.0	1.5	5.0	2.5	148.8	4.2	1.0	0.0

tetraethyl orthosilicate (TEOS; Merck) and $Mg(NO_3)_2{\cdot}6H_2O$ (Merck) were used as received. The starting sol was prepared by hydrolysis of TEOS under magnetic stirring in the presence of 0.1 M HNO_3 (Merck) solution for 60 min while the molar ratio of ($HNO_3 + H_2O$)/TEOS was fixed (TEOS:HNO_3:H_2O = 1:4:16). Subsequently, solutions of $Mg(NO_3)_2{\cdot}6H_2O$ and $Ca(NO_3)_2{\cdot}4H_2O$ were added into the mixture (molar ratio: TEOS:$Mg(NO_3)_2{\cdot}6H_2O$:$Ca(NO_3)_2{\cdot}4H_2O$ = 1:1.44:0.85). The sol was continuously and slowly stirred for 5 h and then kept at 60 °C for overnight to allow gel formation. After 2 days, the resultant translucent gel was dried at 120 °C. The dried gel was heated for 24 h in an electrical box furnace at 700 °C using a heating rate 5 °C min^{-1} to eliminate residual nitrates. Subsequently, powders were heated at 1100 °C, 1300 °C and 1400 °C in the electrical box furnace for 2 h in the none-specified atmosphere. The sol–gel derived powders were milled in a high-speed porcelain mill, and uniaxially pressed to form a cylinder (10 mm × 5 mm). To assess final product bioactivity, merwinite cylinders were sintered at 1300 °C and immersed in SBF for 1, 3, 5, 7, 14 and 28 days at 37 °C. The surface area (sample) to volume (SBF) ratio (SA/V of the SBF solution) was maintained at 0.1 cm^{-1}.

2.2. Preparation of SBF

The SBF solution was prepared by dissolving reagent-grade NaCl, KCl, $NaHCO_3$, $MgCl_2{\cdot}6H_2O$, $CaCl_2$ and KH_2PO_4 in distilled water and buffered at pH = 7.25 with TRIS (trishydroxymethyl aminomethane) and HCl 1 N at 37 °C. Its composition was given in Table 1 and was compared with the human blood plasma composition.

2.3. Sample characterization

2.3.1. X-ray diffraction

The resulting samples were analyzed by X-ray diffraction (XRD) with Philips PW 3710 diffractometer. This instrument was operated with voltage and current settings of 40 kV and 40 mA, respectively and uses Cu Kα radiation (1.540600 Å). For qualitative analysis, XRD diagrams were recorded in the interval $20^\circ \leq 2\theta \leq 70^\circ$ at scan speed of 2° min^{-1} representing the step size of 0.02° and the step time of 1 s.

2.3.2. Fourier transform infra-red spectroscopy

The powder samples were examined by Fourier transform infra-red (FT-IR) with Thermo Nicolet spectrometer. For IR analysis, at first 1 mg of the powder samples was carefully mixed with 300 mg of KBr (infrared grade) and palletized under vacuum. Then the pellet was analyzed in the range of 400–4000 cm^{-1} at the scan speed of 23 scan min^{-1} and the resolution of 4 cm^{-1}.

2.3.3. Differential thermal analysis (DTA) and thermal gravimetric analysis (TGA)

The thermal behavior of the prepared powder was studied by simultaneously thermal analysis (STA). A thermoanalyzer

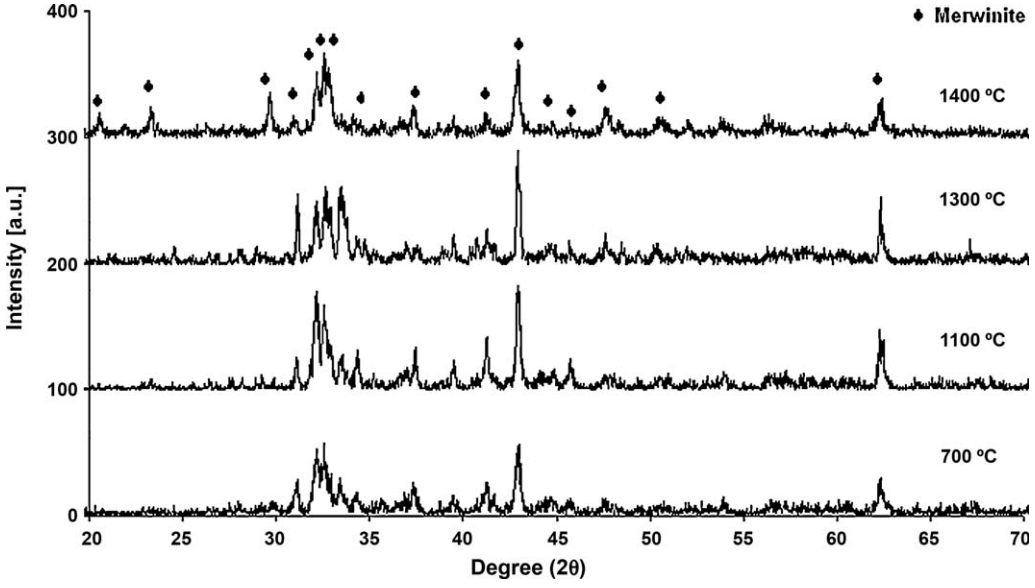

Fig. 1. XRD patterns of the synthesized merwinite.

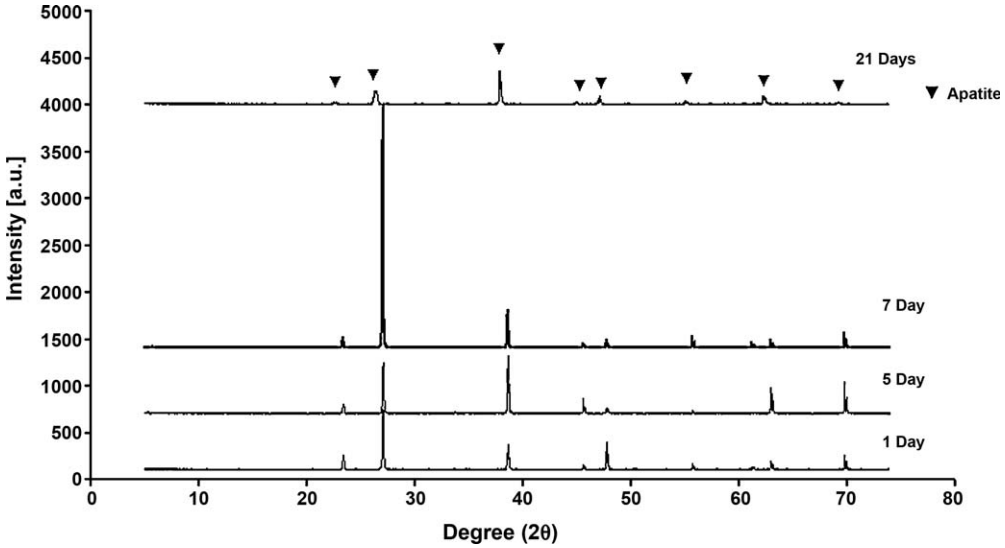

Fig. 2. XRD patterns of the synthesized merwinite after soaking in SBF.

(Netzsch STA 409 PC/PG) that covers the thermal range between ambient temperature and up to 1400 °C with the heating rate of 5 °C min^{-1} was used to record the conventional thermoanalytical curves.

2.3.4. Scanning electron microscope

The samples were coated with a thin layer of gold (Au) by sputtering (EMITECH K450X, England) and then the microstructure of the sample was observed on a scanning electron microscope (SEM; Philips XL 30).

3. Results and discussion

3.1. X-ray diffraction

The XRD patterns of the prepared powder are shown in Fig. 1. XRD results indicate that after calcinations, merwinite is the major phase (PDF No. 25-0161). It is noticeable that while heat treatment at 1100 and 1300 °C caused the crystallinity increased, heating the powder at 1400 °C makes the crystallinity decrease. According to the XRD line-broadening technique and applying the Scherrer equation ($D = k\lambda/\beta \cos\theta$, where k is a constant (shape factor, about 0.9), λ is the X-ray wavelength (1.5405 Å), β is the full width at half maximum (FWHM) of the diffraction line, and θ was the diffraction angle), the mean crystallite sizes D was determined.

The merwinite synthesized at 1300 °C shows crystallite size of approximately 30 nm.

XRD data were also used to confirm the formation of apatite on merwinite bulk after immersion in SBF. XRD results (Fig. 2) indicate a similar standard diffraction pattern that matched JCPDS 9-0432. One should notice that after one day of immersion in SBF apatite peaks emerged and their intensity increase after 5 and 7 days. However after

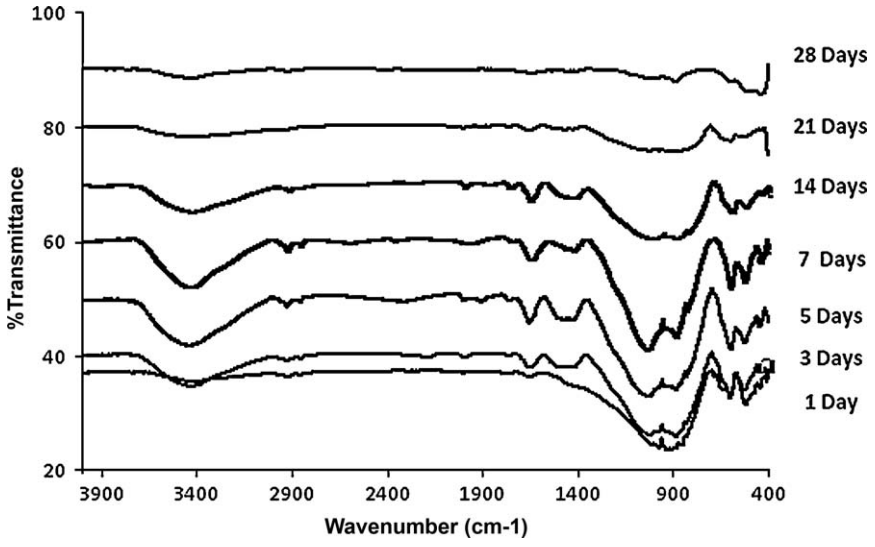

Fig. 3. FT-IR spectra of the synthesized merwinite soaking in SBF for different days.

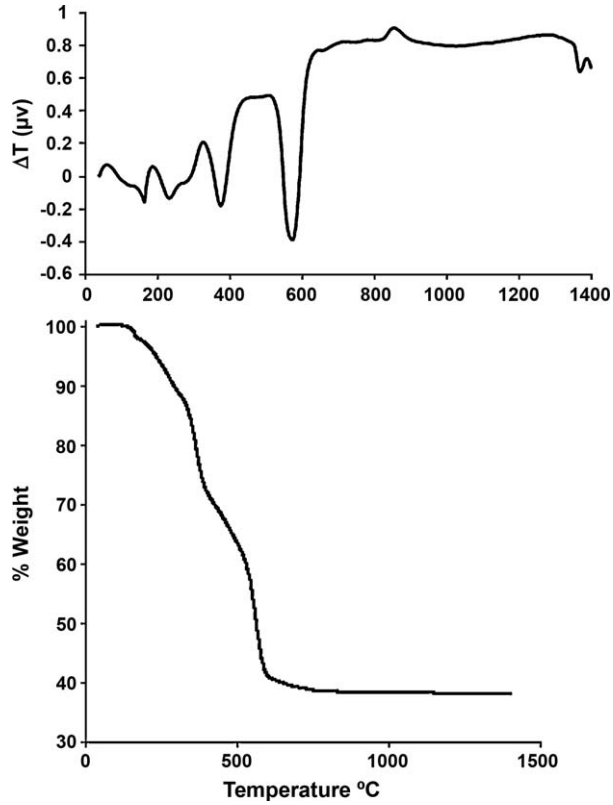

Fig. 4. (a) The DTA and (b) the TGA curves for the synthesized powder.

21 days due to dissolution of apatite layer, intensity of the corresponding peaks decreases.

3.2. Fourier transform infra-red spectroscopy

The essential criteria for a biomaterial to bond with living bone are the formation of a surface apatite layer in the body environment. To determine the apatite formation capacity of this material, the merwinite samples were subjected to *in vitro* solution testing using SBF. Therefore the samples were immersed in SBF while the overall temperature was maintained at 37 °C for 1–28 days. Fig. 3 shows the FT-IR spectra of sample after soaking in SBF for different time span.

The IR spectra of the immersed samples in SBF for 1, 3, 5 and 7 days display following characteristic absorption peaks: (a) the band was observed at 3455 cm^{-1} due to the stretching mode of hydrogen-bonded OH^- ions. (b) The band at 1680 cm^{-1} arises from intercalated H_2O. (c) The band at 1050 cm^{-1} arises from ν_1 PO_4, the band at 895 arises from ν_3 PO_4, the bands at 613 cm^{-1} and 541 cm^{-1} arise from ν_4 PO_4 and finally the band at 450 cm^{-1} arises from ν_2 PO_4. The spectra of the samples showed the similar spectrum with apatite layer; which implies the formation of apatite layer on the surface of the immersed samples. On the other hand, the above mentioned bands disappeared for samples that were soaked in SBF solution for 14, 21 and 28 days. This phenomenon indicated that the formed apatite layer was being dissolved. It is important to pointed out the SBF solution was replaced every day for all samples.

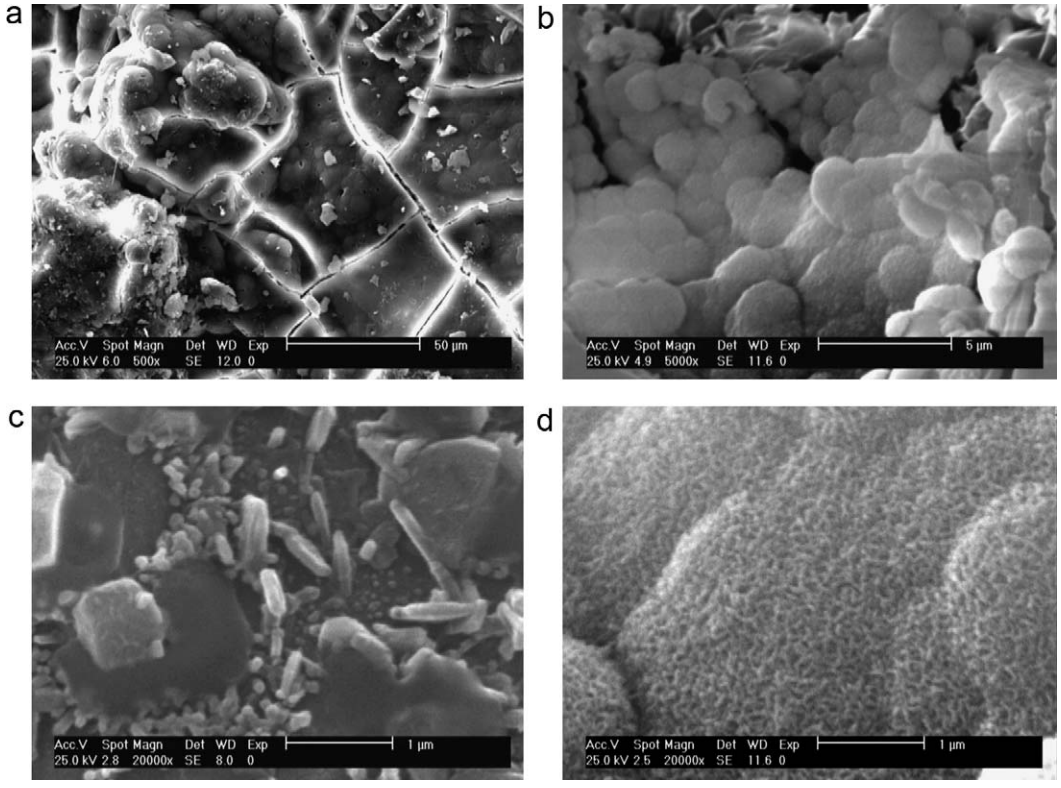

Fig. 5. SEM of the synthesized merwinite samples (a) before, (b) after 1, (c) 7 and (d) 21 days in SBF.

It is notable that the Mg (magnesium) may be able to enter the forming hydroxyapatite nuclei and thus inhibits their evolution to tiny apatite crystals, because this element cannot be accommodated in the hydroxyapatite structure. Mg^{2+} substitute into the apatite lattice causes changes in its physico-chemical properties. Apatite substituted with Mg results in a Ca deficient apatite and may be amorphous calcium phosphate $(Ca,Mg)_9(PO_4)_6$ [35]. In fact, inorganic ions like Mg^{2+} suppress the crystallization of apatite and at higher concentrations favour the formation of amorphous calcium phosphate. These phenomena can promote a greater dissolution of the apatite precipitates in the studied bioactive glass. Therefore, with regards to the above explanation, the XRD patterns indicate some small amounts of hydroxyapatite formation with poor crystallinity meaning that the Bragg peaks are not enough sharp.

3.3. Thermal analysis

The DTA and TGA curves for the synthesized powder are illustrated in Fig. 4a and b, respectively.

Covering the range of 37–600 °C, the obtained result includes three endothermic and one exothermic regions range with peaks at about 130 and 250, 380 and 580 °C. The two first peaks correspond to the dehydration of the precipitated complex and the loss of physically adsorbed water molecules of the merwinite powder. The weight loss in this region was 15%. As the temperature increased two peaks were observed at about 380 and 580 °C, which corresponded to the loss of organics compounds (i.e. alkoxy groups) and the elimination of the residual nitrates introduced as metal nitrate in the preparation of the sol, respectively. The weight loss in this region is 45%. Finally, one exothermic region range was observed at the DTA curve at about 860 °C which was assumed to be the result of crystallization of merwinite powder. These curves confirmed that the residuals could be removed before 700 °C. Also the results from the TGA and DTA analyses allowed us to set the temperature of 700 °C for stabilization of the samples.

3.4. SEM observations

Fig. 5 shows SEM images of the merwinite sample before and after different immersion times. Before soaking, the microstructure includes heterogeneous surfaces consisting of random-sized particles with sharp edges and voids among them.

After 1 day, all samples were completely covered with a newly formed layer. In these micrographs, small particles can be seen which represented crystallization nuclei, after 7 days of soaking, a layer consisting of flake-like particles covered the sample. After 21 days, formed apatite layer start being dissolved which completely dissolved till after 28 days.

4. Conclusion

In conclusion, it can be deduced that the merwinite was successfully synthesized by sol–gel low temperature method and the composition was ensured from the analytical results. Further, the *in vitro* bioactivity analysis in SBF with XRD, FTIR and SEM techniques confirms the growth of hydroxyapatite on the surface of the merwinite ceramics.

Finally, it was found that merwinite samples were compatible for the proposed work in segmental defects in the animal model *in vivo*.

Acknowledgements

This work was supported by Amirkabir University of Technology *(Center of Excellence)* and Research and Clinical Center for Infertility of Yazd. The authors would like to gratefully acknowledge Dr. S. Hesaraki and Mr. H. Barzegar of Materials and Energy Research Center, M. Tahriri and N. Nezafati from Amirkabir University of Technology and M. Abasi-shahni from Islamic Azad University for their contributions to this research.

References

[1] R. Langer, J.P. Vacanti:, Tissue engineering, Science 260 (1993) 920–926.
[2] J.K. Leach, D. Kaigler, Z. Wang, P.H. Krebsbach, D.J. Mooney, Coating of VEGF-releasing scaffolds with bioactive glass for angiogenesis and bone re-generation, Biomaterials 27 (17) (2006) 3249–3255.
[3] W. Liang, N.R. Mohamed, E.D. Delbert, W.M. Nicholas, C.R. Gwendolen, J.M. Jeremy, Bioactive borate glass scaffold for bone tissue engineering, J. Non-Cryst. Solids 354 (15–16) (2008) 1690–1696.
[4] L.L. Hench:, The discovery of bioactive glasses, in: Science, Faith and ethics, Imperial College Press, London, 2001.
[5] L.L. Hench, R.J. Splinter, W.C. Allen, T.K. Greenlee, Bonding mechanisms at the interface of ceramic prosthetic materials, J. Biomed. Mater. Res. 5 (1971) 117–141.
[6] L.L. Hench, Bioceramics, J. Am. Ceram. Soc. 81 (1998) 1705–1728.
[7] C.Y. Kim, A.E. Clark, L.L. Hench, Early stages of calcium phosphate layer formation in Bioglass, J. Non-Cryst. Solids 113 (1989) 195–202.
[8] T. Kokubo, Recent progress in glass-based materials for biomedical application, J. Ceram. Soc. Jpn. 99 (1991) 965–973.
[9] T. Kokubo, H. Kushitani, C. Ohtsuki, S. Sakka, T. Yamamuro, Effects of ions dissolved from bioactive glass–ceramic on surface apatite formation, J. Mater. Sci. Mater. Med. 4 (1993) 1–4.
[10] S.B. Cho, F. Miyaji, T. Kokubo, K. Nakanishi, N. Soda, T. Nakamura, Apatite-forming ability of silicate ion dissolved from silica gels, J. Biomed. Mater. Res. 32 (1996) 375–381.
[11] R. Hill, An alternative view of the degradation of bioglass, J. Mater. Sci. Lett. 15 (1996) 1122–1125.
[12] K.H. Karlsson, Bioactivity of *glass* and its relation to *glass* structure, Glass Phys. Chem. 24 (1998) 280–284.
[13] K.H. Karlsson, R. Backman, M. Hupa, An equilibrium study of phosphate precipitation on bioactive glass, Key Eng. Mater. 218–220 (2002) 103–108.
[14] K.H. Karlsson, Bioactivity of glass and bioactive glasses for bone repair, Glass Technol. 45 (2004) 157–161.
[15] S. Agathopoulosa, D.U. Tulyaganova, J.M.G. Ventura, S. Kannana, M.A. Karakassides, J.M.F. Ferreira, Formation of hydroxyapatite onto glasses of the $CaO–MgO–SiO_2$ system with B_2O_3, Na_2O, CaF_2 and P_2O_5 additives, Biomaterials 27 (9) (2006) 1832–1840.
[16] L.L. Hench, Bioceramics, J. Am. Ceram. Soc. 81 (1998) 1705–1728.
[17] P. Siriphannon, Y. Kameshima, A. Yasumori, K. Okada, S. Hayashi, Influence of preparation conditions on the microstructure and bioactivity of $CaSiO_3$ ceramics: formation of hydroxyapatite in simulated body fluid, J. Eur. Ceram. Soc. 22 (2002) 511–520.
[18] X.Y. Liu, C.X. Ding, P.K. Chu, Mechanism of apatite formation on wollastonite coatings in simulated body fluids, Biomaterials 25 (2004) 1755–1761.
[19] X.Y. Liu, C.X. Ding, Z. Wang, Apatite formed on the surface of plasma-sprayed wollastonite coating immersed in simulated body fluid, Biomaterials 22 (2001) 2007–2012.

[20] P.N. De Aza, Z.B. Luklinska, M.R. Anseau, F. Guitian, S. De Aza, Bioactivity of pseudowollastonite in human saliva, J. Dent. 27 (1999) 107–113.
[21] C. Sarmento, Z.B. Luklinska, L. Brown, M. Anseau, P.N. De Aza, S. De Aza, et al., In vitro behavior of osteoblastic cells cultured in the presence of pseudowollastonite ceramic, J. Biomed. Mater. Res. A 69 (2004) 351–358.
[22] P.N. De Aza, Z.B. Luklinska, A. Martinez, M.R. Anseau, F. Guitian, Morphological and structural study of pseudowollastonite implants in bone, J. Microsc. 197 (2000) 60–67.
[23] P.N. De Aza, Z.B. Luklinska, M.R. Anseau, F. Guitian, S. DeAza, Transmission electron microscopy of the interface between bone and pseudowollastonite implant, J. Microsc. 201 (2001) 33–43.
[24] P.N. De Aza, A.H. De Aza, A. Herrera, F.A. Lopez-Prats, P. Pena, Influence of sterilization techniques on the in vitro bioactivity of pseudowollastonite, J. Am. Ceram. Soc. 89 (2006) 2619–2624.
[25] T. Nonami, S. Tsutsumi, Study of diopside ceramics for biomaterials J, Mater. Sci. Mater. Med. 10 (1999) 475–479.
[26] P.N. De Aza, Z.B. Luklinska, M.R. Anseau, Bioactivity of diopside. Ceramic in human parotid saliva, J. Biomed. Mater. Res. B 73 (2005) 54–60.
[27] N.Y. Iwata, G.H. Lee, Y. Tokuoka, N. Kawashima, Sintering behavior and apatite formation of diopside prepared by coprecipitation process, Colloids Surf. B: Biointerfaces 34 (2004) 239–245.
[28] W.Y. Zhao, J. Chang, Preparation and characterization of novel tricalcium silicate bioceramics, J. Biomed. Mater. Res. A 73 (2005) 86–89.
[29] R.L. Du, J. Chang, Preparation and characterization of bioactive sol–gel-derived $Na_2Ca_2Si_3O_9$, J. Mater. Sci. Mater. Med. 15 (2004) 1285–1289.
[30] C.T. Wu, J. Chang, Synthesis and apatite-formation ability of akermanite, Mater. Lett. 58 (2004) 2415–2417.
[31] C.T. Wu, J. Chang, A novel akermanite bioceramic: preparation and characteristics, J. Biomater. Appl. 21 (2) (2006) 119–129.
[32] C.T. Wu, J. Chang, S.Y. Ni, J.Y. Wang, In vitro bioactivity of akermanite ceramics, J. Biomed. Mater. Res. A 76 (2006) 73–80.
[33] E.S. Larsen, W.F. Foshag, Merwinite, a new calcium magnesium orthosilicate from Crestmore, California, Amer. Mineral. 6 (1921) 143–148.
[34] J. Ou, Y. Kang, Z. Huang, X. Chen, J. Wu, R. Xiao, G. Yin, Preparation and in vitro bioactivity of novel merwinite ceramic, Biomed. Mater. 3 (2008) 015015 (8pp).
[35] A. Martinez, I. Izquierdo-Barba, M. Vallet-Regi, Bioactivity of a CaO–SiO_2 binary glasses system, Chem. Mater. 12 (2000) 3080–3088.